Devolatilization kinetics from entrained flow reactor experiments: evaluation of scenario uncertainties through CFD modelling

Chiara Galletti,* Gianluca Caposciutti, and Leonardo Tognotti

Department of Civil and Industrial Engineering, University of Pisa, Italy

E-mail: chiara.galletti@unipi.it

Abstract

A Computational Fluid Dynamic model of oxy-coal devolatilization experiments in a pilot-scale entrained flow reactor is proposed to gain insight into the thermal histories of the cloud of solid fuel. Particles experience different paths and are characterized by a temperature which is lower than the reactor one at most of the locations used for sampling. Indeed, assuming the particles to be at the reactor temperature, leads to devolatilization kinetics that strongly underestimate conversion. However, a simple assumption on a linear dependence of the particle temperature on the residence time through an average heating rate, with residence time and heating rate estimated from the numerical model, was found to largely improve devolatilization kinetics even when using a simple Single First Order Model. Variances of residence time and heating rate in the particle cloud were used to evaluate uncertainties on predicted conversions and kinetic parameters.

Introduction

It is believed that coal will still play a significant role in future for electric power generation because of its low cost and abundance. However the use of coal demands for new technologies able to limit pollutants and ensure a strong reduction of greenhouse gas emissions through Carbon Capture and Sequestration (CCS). One option is to consider oxy-coal combustion, in which a mixture of oxygen and recycled flue gases is used instead of air for coal oxidation[1]. Consequently, a gas consisting of CO_2 and H_2O is obtained, with a CO_2 concentration ready for sequestration. Flue gases are recycled in order to make up the volume of the missing N_2 and to ensure enough thermal capacity for the subsequent heat transfer operations. All comprehensive reviews on oxy-coal combustion[1,2,3] highlight the need of better understanding the changes in coal combustion characteristics with respect to conventional operations, due to the different atmosphere in which combustion takes place. Indeed the availability of sub-models able to describe the different steps of the coal combustion process (devolatilization, char oxidation, etc.) may strongly improve the reliability of modeling tools, usually based on Computational Fluid Dynamics (CFD), which are considered essential for the development of new combustion technologies. The key issue is that most of the available models have been derived for conventional combustion and should be validated and eventually revised for oxy-fuel conditions[4].

Such understanding on the coal combustion process should be gained through experiments carried out in facilities able to ensure operating conditions similar to the ones encountered in industrial furnaces, where the pulverized coal is heated up quickly to high temperatures, and completes devolatilization in a short residence time, loosing from 20 to 60% of its initial mass. Hence, flame characteristics (e.g. flame front position and stability, combustion efficiency) are partly governed by the volatile release; the comprehension of devolatilization kinetics thus constitutes a first steps towards the investigation of the entire coal combustion process.

The conventional analysis of devolatilization with thermogravimetry on lab-scale can only

give a fingerprinting of the fuel, because the thermal conditions are far from those of practical applications[5]; for instance devolatilization kinetics change substantially when varying the heating rate.

In this framework, entrained flow reactors (EFRs) are appealing as they are able to approximate the main characteristics of industrial furnaces, in terms of heating rates and temperatures. For instance, Li et al.[6], designed EFR experiments to emulate the pulverized coal injection system of an ironmaking blast furnace. Different analyses can be carried out on the gaseous products and solid residues; hence EFRs are frequently used for determining solid fuel conversions in specific operating conditions. Some authors used both thermogravimetry and EFR experiments for the characterization of oxy-coal combustion, highlighting the importance of the char-CO_2 reactions[7,8]. Shaddix and Molina[9] and Galletti et al.[10] used EFRs to investigate the coal ignition delay and concluded that the higher molar heat capacity of CO_2 than N_2 leads to larger ignition delays in oxy-fuel than in conventional conditions. EFRs have been recently utilized to investigate PM10 formation in oxy-fuel conditions[11] as well as the chemical composition of sub-micrometer particulate matter PM1[12,13]. Similarly Chen et al.[14] used EFRs to investigate the particle size evolution during pulverized coal combustion in oxy-fuel conditions, showing that devolatilization in CO_2 produces finer char particles than that in N_2. Recently Wang et al.[15] performed EFR experiments to investigate formation of NO and char characteristics in oxy-coal combustion.

EFRs could potentially provide insight into kinetics but only with the aid of sophisticated experimental techniques (requiring an optical access to the EFR interior[16],[17]) or tedious procedures to determine the effective particle thermal history. For instance Ballester and Jiménez developed a model for the particle combustion and used experimental conversion to search for the best kinetic parameter of a Single First Order Reaction devolatilization model[18]. They evidenced the presence of a certain range of kinetic parameters able to satisfactorily predict the experimental conversions.

Indeed, kinetics are usually derived by assuming a constant particle temperature (equal to

the reactor one), hence neglecting the very quick heating up of the solid fuel particles. However, this procedure may induce some errors especially when considering devolatilization, which occurs in very short residence times, comparable with the time-scale of the heating process. Hence, the present work wants to investigate whether the use of CFD modeling to estimate the particle thermal histories may improve the accuracy of the estimated kinetics. Indeed, recently a few studies applied CFD to the analysis of EFRs. Simone et al. used CFD to model a lab-scale EFR, suggesting to use predicted thermal histories for evaluating biomass devolatilization kinetics[19,20]. Alvarez et al. developed a CFD model of a EFR to study the coal combustion behavior under O_2/CO_2 conditions, showing, with respect to air combustion, a decrease in the predicted peak temperature and a reduction in coal burnout rate[21]. The authors highlighted the need for oxy-fuel kinetics.

Vascellari at al. investigated different devolatilization models and suggested an iterative procedure, based on CFD analysis of the EFR to better calibrate the parameters of the models[22], highlighting the importance of taking into account the particle heating. Jovanovic at al. studied the ignition point of pulverized coal flames in oxy-fuel conditions, developing a CFD model of a EFR[23]. They used different devolatilization models and observed a better performance of the Functional Group model that of a simple Single-First-Order Reaction model; however the former resulted to be very computational demanding is CFD simulations. The authors also stated that all devolatilization models loose their accuracy for very low oxygen fraction at low oxidant temperatures, and at very high oxidant temperatures. Very recently Li et al. suggested to use CFD to better derive biomass devolatilization kinetics from EFR experiments[24]. They proposed an iterative procedure to optimize the parameters of a two-competing-rates devolatilization model by taking information on particle temperature from the CFD simulations.

The present work proposes CFD modeling to improve the knowledge of a pilot scale entrained flow reactor with the ultimate goal of driving the procedures for deriving kinetics. The objective is also to evaluate some possible sources of uncertainties and their ultimate

effect on the kinetic parameters. To accomplish that, a multi-level numerical modeling and experimentation is proposed, and the matching between predicted and measured conversion data is carried out by taking into account both CFD and experimental error bars. Importantly, only a few works in literature attempted to evaluate uncertainties on experimental measurements[17,25,26,27] or modeling parameters[18] in entrained flow reactors.
The approach will be shown to derive simple devolatilization kinetics in oxy-coal conditions; however it can be potentially applied to more complex devolatilization schemes, different solid fuels (i.e. biomass) as well different atmospheres.

Test case

The entrained flow reactor

The investigated entrained flow reactor is called Isothermal Plug Flow Reactor, and belongs to the International Flame Research Foundation (IFRF). It is sited in the Experimental Area of ENEL Ricerca in Livorno, Italy. A scheme of the EFR is shown in Figure 1.

[Figure 1 about here.]

[Figure 2 about here.]

The reactor allows testing solid fuels under conditions similar to industrial applications with high temperatures ($1000 - 1600$ K) and heating rates (10^4-10^5 K/s)[28,29]. The reactor inner tube is 4.5 m long with a diameter of 0.15 m. At the walls, nine modules with electric resistances keep the temperature at a set point value. Each module has several ports which are available for coal injection or for the insertion of measuring instruments. Pulverized fuel particles are transported by a carrier gas (nitrogen/air) and injected from a side through a radial probe (with an inner diameter of 0.7 cm and curved at the edge to allow an axial injection, see Figure 2) into a flue gas stream and move along the reactor. Flue gases come from a pre-heating combustion section which supplies gases of desired composition

and temperature. Moreover flue gases can be mixed with an additional diluent (such as nitrogen) to control the temperature of the gas stream. Several type B thermocouples are inserted in the main EFR tube to monitor the temperature along the reactor. At the reactor bottom, flue gas and particles are quenched down to 500 K with nitrogen and then treated in a separation and analysis system made of two cyclones and a bag filter, before being discharged in to the atmosphere.

Experimental data

The experimental runs considered in the present work regard devolatization, even though also char oxidation tests were performed. Devolatilization tests were run in absence of oxygen with residence times in the range 25-250 ms. The coal is Sebuku Indonesian coal with proximate and ultimate analysis reported in Table 1.

[Table 1 about here.]

The coal was sieved to a dimensional range 63-90 μm and laser diffractometry was used to determine the particle size, which was fitted by a Rosin-Rammler distribution

$$F_m(d_P) = 1 - exp[(\frac{d_p}{\delta})^n] \tag{1}$$

with $\delta = 99.46$ μm and $n = 5.46$. Particles exiting the EFR are sampled and analyzed through thermogravimetry in order to obtain the ash content, and thus to determine the conversion as:

$$X = (1 - \frac{ash_0}{ash}) \cdot 100 \tag{2}$$

Devolatilization runs were performed using three different nominal temperatures, namely $T_R = 1173, 1373$ and 1573 K in absence of oxygen and using CO_2 as carrier gas in order to emulate oxy-fuel conditions. Flow rates are given in Table 2.

[Table 2 about here.]

Methodology

CFD modelling was performed with different levels of complexity in order to gain insight into specific flow features. Hence, different simulations were carried out, corresponding to:

1. single-phase flow;
2. injection of inert particles;
3. injection of reacting particles.

The approach is depicted in the scheme of Figure 3.

[Figure 3 about here.]

In step 1, simulations of the single-phase flow, i.e. in absence of any particles, are carried out to allow understanding the gas flow and temperature field. In this case predicted temperatures are compared to available temperature measurements inside the reactor. In step 2, inert particles are injected numerically in the reactor in order to observe the cloud of particles. The coefficient of restitution describing the particle-wall interaction was found to play a strong role in determining the shape of the solid particle jet. Such simulations are compared with a visual observation of the shape of the feeding jet from the probe, although taken in open air. The lack of optical access in the EFR prevented from observing the jet directly in the reactor. Finally, in step 3 reacting coal particles are injected in the reactor. The idea is to gain insight into the thermal histories that are experienced by the particles in order to guide the approach for calculating devolatilization kinetics. The comparison between modelling results and experimental data on conversion allows assessing the performance of the devolatilization models.

Numerical model

The rector model was developed with the commercial CFD code Fluent® by ANSYS Inc.. The grid was generated with the software ICEM. Just half EFR was modeled because of its

geometric symmetry. In order to avoid creating one geometry and grid for each experimental run, the chosen domain referred to the run with the largest reactor length (i.e. distance between feeding pipe and sampling probe) and a post-processing procedure was developed on purpose to emulate the different positions of the sampling probe. The grid was unstructured and refined near the feeding and sampling probes. A grid independence study was performed on the velocity field using a number of cells raging from 700k to 1.5M; the chosen grid consisted of 900k cells. Reynolds-averaged Navier-Stokes equations were solved for step 1 using the standard and RNG $\kappa - \epsilon$ turbulence model[30].

A one-way coupled Lagrangian tracking was adopted for step 2, because of the low volumetric fraction of the solid particles. About 1600 particle tracks were followed in the domain. Runs were performed using different coefficients of restitution. The coefficient of restitution describes the particle-wall interaction: the normal coefficient represents the amount of momentum in the direction normal to the wall that is retained by the particle after the collision with the wall; similarly the tangential coefficient defines the amount of momentum in the direction tangential to the wall that is retained by the particle. The normal and tangential coefficients of restitution were taken to be equal and three different values were investigated, i.e. $R = 0.3$, 0.6 and 1.

Finally a two-way coupled Lagrangian tracking was adopted for step 3. Devolatilization was modeled using a Single First Order Rate (SFOR), that assumes that the rate of devolatilization is first-order dependent on the amount of volatiles remaining in the particle.

$$\frac{\partial VM_p}{\partial t} = -k(VM_\infty - VM_p) \tag{3}$$

where VM_p and VM_∞ are the actual and maximum volatile matter content of the particle. k is the kinetic rate, that is defined by input of an Arrhenius type pre-exponential factor A and an activation energy E.

$$k = Ae^{-\frac{E}{RT}} \tag{4}$$

VM_∞ can be evaluated from the high temperature volatile yield, that for the coal under investigation and resulted to be 1, 1.2 and 1.38 for $T_R = 1173, 1373$ and 1573 K runs, respectively. The volatiles oxidation was represented by 2-step schemes as:

$$C_{1.04}H_{3.16}O_{0.83}N_{0.0634}+0.89\ O_2 \rightarrow 1.04\ CO + 1.58\ H_2O + 0.0317\ N_2 \text{ at } 1173\ K$$
$$C_{1.29}H_{2.82}O_{0.74}N_{0.0566}+0.93\ O_2 \rightarrow 1.20\ CO + 1.41\ H_2O + 0.0283\ N_2 \text{ at } 1373\ K$$
$$C_{1.37}H_{2.45}O_{0.64}N_{0.0492}+0.97\ O_2 \rightarrow 1.37\ CO + 1.22\ H_2O + 0.0246\ N_2 \text{ at } 1573\ K$$
$$CO+0.5O_2 \rightarrow CO_2$$

The Eddy Dissipation Model was used to treat the turbulence-chemistry interaction[31]. Radiation was taken into account through the P1 radiation model and Weighted Sum of Gray Gases Model (WSGG) for the spectral properties with coefficients from Smith et al.[32]. The particle emissivity was 0.7.

A stationary solver was used to solve the equations using a second order discretization scheme and the SIMPLE algorithm for the pressure-velocity coupling. The steadiness of the solution with iteration was checked for convergence. All residuals were well below 10^{-4}.

Post-processing

As mentioned in the Introduction, in order to avoid creating one geometry and one mesh for each experimental run, the chosen domain referred to the run with the largest reactor length. Subsequently an Matlab® program was written to vary virtually the position of the sampling probe in order to select only the particles which would be effectively sampled and carry on the subsequent analysis just on them. Data on particle position, temperature and volatiles concentration, for all the 1600 particles inside the reactor, were extracted from the CFD simulations and analyzed by the program. This basically checks the position of the particles and considers only the ones that are located at a distance from the feeding probe equal to the reactor length (position of the sampling probe) of the selected experimental run. Then, only the particles placed at a radial coordinate lower than the sampling probe

diameter are selected. For these particles, the thermal history and conversion are calculated. The former is used to evaluate the heating rate and may help the derivation of kinetics[19], whereas the conversion is compared to the experimental one. The procedure is shown in Figure 4.

[Figure 4 about here.]

Results

Single-phase

The single-phase runs allow gaining insight into the temperature field in the EFR and assessing the hypothesis of uniform temperature field, often made in EFR studies. Figure 5 shows the comparison of predicted and experimental temperatures at different distances from the feeding probe.

[Figure 5 about here.]

It can be observed that the temperature minimum is not placed in the reactor axis but it is shifted towards the feeding probe side. This is evident from both the measured and predicted data, although predictions indicated a lower value of the minimum temperature. The reason may be imputed to the shape of the feeding probe. Figure 6 shows the distribution of temperature in the longitudinal mid-plane of the reactor for a nominal temperature T_R=1373 K, the carrier gas cold jet is not aligned with the reactor axis. It can be also observed from the temperatures near the walls that these match well the value of the nominal reactor temperature, whcih is set during the experiments.

[Figure 6 about here.]

Inert particles

As mentioned in Section , the injection of inert particles was aimed at evaluating the effect of some numerical parameters on the results. In particular the particle coefficient of restitution, R, describing the particle-wall interaction, plays a fundamental role in determining the shape of jet of particles released from the feeding probe. This occurs mainly because injected coal particles impact on the feeding pipe walls (especially those corresponding to the bend before injection) due to their inertia and this affects the shape of the jet.

Figure 7a shows the results of a simple experiment aimed at clarifying the shape of the jet. Figures 7b-d report also particle tracks colored by their diameter as predicted using different coefficient of restitution. It can be noticed that restitution coefficients of $R = 0.3$ and $R = 0.6$ provide a shape of the jet which is in good agreement with the experimental picture, whereas $R = 1$ provides a jet which is too spread. Therefore it was chosen to use $R = 0.3$, value which can also be found in literature[33].

[Figure 7 about here.]

It is clear that coal particles experience different thermal histories due to their distinct velocities and positions in the reactor. Figure 8a,c,e shows the particle thermal histories predicted using inert particle simulations at different reactor temperatures. It is well evident the spread of thermal behaviors. For the same distance y from the feeding nozzle, the particles exhibit also different residence times t, due to their distinct trajectories, as reported in Figure 8b,d,f.

The cloud of coal particles can be analyzed in term of mean and standard deviation. The second and third columns of Table 3 report average value and standard deviation of heating rates, HR, as calculated for the inert particles for different reactor temperatures. It can be observed that the estimated HR has a standard deviation of about 10-20 % of its absolute value. Similarly Table 4 lists average and standard deviation of residence times, t, predicted with the inert particle simulations.

[Figure 8 about here.]

[Table 3 about here.]

[Table 4 about here.]

Reactive particles

Some considerations arise from the previous sections. Firstly, experimental runs were planned by estimating the position of the sampling probe with respect to the feeding one, as the mean gas speed velocity multiplied by the desired residence time. The mean gas velocity was evaluated from the flue gas flow rate. However previous section clearly shows that particles are characterized by a distribution of residence times, that are likely to be different from the flue gas one. Secondly, the procedure to derive kinetics from conversion data in EFR experiments should be revised. Usually, the particle temperature is assumed to be constant and equal to the reactor nominal temperature. However devolatilization is a quick phenomenon; therefore, one may expect that the coal particles have not reached the reactor temperature at the position chosen for sampling. Things are further complicated by the fact that not all the particles behave in the same manner.

Hence, the present work wants to show some sources of errors that may arise when deriving kinetics from EFR experiments, related to treatment of the particle residence time, t, and temperature, T_p. Indeed, as mentioned in the Introduction, the idea is to use CFD simulations to evaluate t and T_p data, highlighting their uncertainties and how they affect kinetic calculations.

Two different procedures to derive a simple Single First Order Reaction (SFOR) model were considered and these will be denoted as *SFOR* and *SFOR-HR*. In case of constant temperature of the particle (equal to the reactor temperature T_R) the SFOR model given in Equation 3 can be solved to give:

$$VM_p(t) = VM_\infty e^{-kt}. \tag{5}$$

If experimental data on final volatile matter are available (VM_{exp}) for J sampling residence times, a linear regression can be performed to evaluate the kinetic constant k_i from the runs at the i-th reactor temperature:

$$\frac{\sum_{j=1}^{J} \frac{ln\frac{VM_{\infty,i}}{VM_{exp,j}}}{t_j}}{J} = k_i \tag{6}$$

This procedure can be made for different reactor temperatures, in order to evaluate the Arrhenius parameters, A and E as:

$$lnk_i = -\frac{E}{R}\frac{1}{T_i} + lnA \tag{7}$$

This will be denoted as *SFOR* model. However, since the present results indicate that coal particles may not reach the reactor nominal temperature for all sampling positions, it was chosen to consider that particle temperature is not constant and equal to the reactor one. In particular the particle thermal histories were assumed to be characterized by a temperature increase proportional to the residence time t through the heating rate HR:

$$T_p(t) = T_0 + HR \cdot t; \quad HR = \frac{\partial T}{\partial t} \tag{8}$$

where T_0 is the injection temperature. Hence Equation 3 is solved using Equation 8 to determine the particle temperature:

$$\int_0^t \frac{\partial VM_p}{\partial t} dt = \int_0^t -Aexp(-\frac{E}{R(HR \cdot t + T_0)})(VM_\infty - VM_p)dt \tag{9}$$

The analytic solution is:

$$\begin{aligned} VM_p(t) = VM_\infty exp[-\frac{AE}{R \cdot HR}(EI(-\frac{E}{R(T_0 + HR \cdot t)}) + \\ + \frac{R(T_0 + HR \cdot t)}{E} exp(-\frac{E}{R(T_0 + HR \cdot t)}) - EI(-\frac{E}{RT_0}) - \frac{RT_0}{E} exp(-\frac{E}{RT_0}))] \end{aligned} \tag{10}$$

where EI is the infinite exponential. A best fitting procedure can then be carried out to find the kinetic parameters A and E. Considering J samples taken at I reactor temperatures, an objective function was developed using the experimental volatile matter VM_{exp} and predicted heating rate, HR, and residence time t.

$$\begin{cases} (A,E) \Longleftrightarrow min\sqrt{\sum_{i=1}^{I}\sum_{j=1}^{J}[VM_{analytic}(HR_i,t_{i,j}) - VM_{exp,i,j}]^2} \\ E_{min} \leq E \leq E_{max} \qquad E_{min} > 0 \\ A_{min} \leq A \leq A_{max} \qquad A_{min} > 0 \end{cases} \tag{11}$$

A constrained minimization was performed using interior point algorithm. Initial guess value and solution method were found to not affect significantly A and E evaluation. The model will be called *SFOR-HR*.

Both SFOR and SFOR-HR devolatilization models return A and E kinetic coefficients that can be implemented easily in the devolatilization reaction in the CFD model of the EFR. These parameters are reported in the third and sixth column of Table 5. It can be observed that the activation energy is five times higher with the SFOR model than the SFOR-HR, thus indicating a larger dependence on temperature of k. This is depicted through solid lined in Figure 9. Hence, neglecting the particle heating region, by assuming a constant particle temperature equal to the maximum (i.e. reactor) one, leads to kinetics strongly dependent on temperature; conversely, taking into account the heating up of solid fuel, smooths the dependence of kinetics on temperature.

[Table 5 about here.]

[Figure 9 about here.]

The residence times of the sampled solid fuel particles as a function of reactor length are shown in Figure 10 for both SFOR and SFOR-HR model, at the three different reactor temperatures. It can be noticed a large variation of residence times, with the presence

also a few particles characterized by higher times due to deviation in their trajectory. The expected residence time based on the average gas flow rate is also reported for comparison; a preliminary evaluation of residence time appears affected by errors and difficult to be calculated without CFD simulations.

[Figure 10 about here.]

Figure 11 shows particle thermal histories as obtained from simulations performed using the SFOR and SFOR-HR models. It can be observed that thermal histories are affected by the devolatilization model; in particular the spread of thermal histories is larger with the SFOR model than with the SFOR-HR model. It can be also observed the presence of a few particles with a weird behavior due to particular trajectories, affected by recirculation regions.

[Figure 11 about here.]

Heating rate HR and residence time t values calculated for the two models at the three reactor temperatures are reported in Table 3 and 4, respectively for inert and reacting particles with SFOR and SFOR-HR devolatilization models. The residence times of the inert particles are always lower than those of the reacting particles due to the higher inertia, whereas the heating rates differ from those from the reacting particles by of 10% at maximum.
Comparison between experimental conversions and those predicted by the SFOR and SFOR-HR models at different residence times are reported in Figure 12 for all three reactor temperatures. Vertical error bars on the experimental values were obtained by considering an uncertainty of 0.1% on the determination of the ash content, whereas the experimental horizontal bars were derived by considering an uncertainty of 1 cm on the probe position, The error bars on the predicted data are related to the cloud of particles: horizontal bars represent the variance associated with the residence time, whereas vertical bars represent the

variance associated with the volatile matter content in the group of particle.

The SFOR model was found to systematically under-predict the conversion rates whereas a strong improvement was achieved by taking into account a non uniform particle temperature when calculating the kinetic parameters.

Results with the SFOR-HR model are in very good agreement with experimental conversion data at $T_R = 1173K$ and $1373K$, whereas discrepancies are present at the highest temperature. However the $T_R = 1573K$ data set was the one with the largest uncertainties, also from the experimental point of view. This is also evident from the non monotonic trend of the conversion with respect to residence time.

Hence the revision of the procedure to derive devolatilization rates from EFRs may improve strongly the matching between modeling and experiments thus providing more reliable kinetics.

[Figure 12 about here.]

The standard deviations on heating rate σ_{HR} and residence time σ_t reported in Tables 3 and 4, respectively, represent the variations in heating rate and residence time experienced by the coal particles because of their different trajectories. Hence standard deviations may provide additional information to characterize the cloud of particles, in addition to the average heating rate HR and residence time t.

A preliminary and rough estimation on how uncertainties on HR and t affect the SFOR kinetic parameters was performed by re-computing A and E, with $t \pm \sigma_t$ and then $HR \pm \sigma_{HR}$ separately. Results are reported in Table 5 and depicted in Figure 9. It can be noticed that residence times are more influent than heating rate variations on kinetics evaluation.

Conclusions

A numerical model of a pilot-scale entrained flow reactor was developed to aid experimental campaigns on oxy-coal combustion by providing an estimation of the particle thermal histo-

ries, needed for deriving kinetics.

Both experiments and CFD models were planned and performed with different levels of complexity, including the analyses of the single-phase reactor thermal field, the jet of non-reacting particles and finally the jet of the reacting solid fuel. CFD modeling is an efficient way to shed light into the whole solid fuel cloud, provided that attention is made to some modeling parameters such as the coefficient of restitution describing the particle-wall interaction, which affects substantially the shape of the solid fuel jet.

Coal particles injected in a EFR experience different paths and thermal histories; moreover they were observed to be at a temperature lower than the reactor one at most of the sampling positions used for the devolatilization tests. Similar conclusion was also recently drawn by Li et al.[24] on biomass devolatilization in an EFR.

These findings suggested to revise the way kinetics are calculated. Firstly residence times were derived from CFD calculations, as a preliminary estimation is difficult and inaccurate. Secondly, the temperature of the particles was considered to be different from the reactor one by fitting the average thermal history with a linear function, thus considering the average heating rate from the CFD model. In this manner the volatile release equation described by a low cost SFOR model could be integrated analytically.

This procedure was found to largely improve the agreement between experimental and predicted conversion data. Conversely, the assumption of a constant particle temperature leads to a significant underestimation of the kinetic rates, especially at the lower temperatures, and hence of the predicted conversions.

Finally, the cloud of particles was taken into account through averages and standard deviation of the variables of interest, i.e. residence time and heating rate. These data can be used to estimate uncertainties on predicted conversion as well as on the final kinetic parameters. Hence this work wants to provide a first attempt to estimate uncertainties on kinetic derivation from entrained flow reactor data. Although the investigated coal was characterized by a narrow range of size, further efforts should be devoted to the analysis of particle size effects

on the determination of kinetics.

References

(1) Wall, T.; Liu, Y.; Spero, C.; Elliott, L.; Khare, S.; Rathnam, R.; Zeenathal, F.; Moghtaderi, B.; Buhre, B.; Sheng, C.; Gupta, R.; Yamada, T.; Makino, K.; Yu, J. *Chemical Engineering Research and Design* **2009**, *87*, 1003 – 1016.

(2) Toftegaard, M. B.; Brix, J.; Jensen, P. A.; Glarborg, P.; Jensen, A. D. *Progress in Energy and Combustion Science* **2010**, *36*, 581 – 625.

(3) Chen, L.; Yong, S. Z.; Ghoniem, A. F. *Progress in Energy and Combustion Science* **2012**, *38*, 156 – 214.

(4) Galletti, C.; Coraggio, G.; Tognotti, L. *Fuel* **2013**, *109*, 445–460.

(5) Authier, O.; Thunin, E.; Plion, P.; Porcheron, L. *Energy and Fuels* **2015**, *29*, 1461–1468.

(6) Li, H. b.; Elliott, L.; Rogers, H.; Wall, T. *Energy and Fuels* **2014**, *28*, 363–368, cited By 3.

(7) Meng, F.; Yu, J. b.; Tahmasebi, A.; Han, Y. *Energy and Fuels* **2013**, *27*, 2923–2932.

(8) Naredi, P.; Pisupati, S. *Energy and Fuels* **2011**, *25*, 2452–2459, cited By 14.

(9) Shaddix, C. R.; Molina, A. *Proceedings of the Combustion Institute* **2009**, *32*, 2091 – 2098.

(10) Galletti, C.; Giacomazzi, E.; Giammartini, S.; Coraggio, G.; Tognotti, L. *Energy and Fuels* **2013**, *27*, 2732–2740.

(11) Wen, C.; Yu, D.; Wang, J.; Wu, J.; Yao, H.; Xu, M. *Energy and Fuels* **2014**, *28*, 5682–5689.

(12) Kazanc, F.; Levendis, Y. *Energy and Fuels* **2012**, *26*, 7127–7139.

(13) Kazanc, F.; Levendis, Y.; Maffei, T. *Energy and Fuels* **2013**, *27*, 4984–4998, cited By 5.

(14) Chen, Y.; Wang, G.; Sheng, C. *Energy and Fuels* **2014**, *28*, 136–145, cited By 3.

(15) Wang, G.; Zander, R.; Costa, M. *Fuel* **2014**, *115*, 452 – 460.

(16) Lemaire, R.; Bruhier, C.; Menage, D.; Therssen, E.; Seers, P. *Journal of Analytical and Applied Pyrolysis* **2015**, –.

(17) Tolvanen, H.; Raiko, R. *Fuel* **2014**, *124*, 190–201.

(18) Ballester, J.; Jimnez, S. *Combustion and Flame* **2005**, *142*, 210 – 222.

(19) Simone, M.; Biagini, E.; Galletti, C.; Tognotti, L. *Fuel* **2009**, *88*, 1818 – 1827.

(20) Simone, M.; Marcucci, M.; Biagini, E.; Galletti, C.; Tognotti, L. *Chemical Engineering Transactions* **2009**, *17*, 181–186.

(21) lvarez, L.; Gharebaghi, M.; Jones, J.; Pourkashanian, M.; Williams, A.; Riaza, J.; Pevida, C.; Pis, J.; Rubiera, F. *Applied Energy* **2013**, *104*, 653 – 665.

(22) Vascellari, M.; Arora, R.; Pollack, M.; Hasse, C. *Fuel* **2013**, *113*, 654 – 669.

(23) Jovanovic, R.; Milewska, A.; Swiatkowski, B.; Goanta, A.; Spliethoff, H. *Fuel* **2012**, *101*, 23 – 37, 8th European Conference on Coal Research and Its Applications.

(24) Tian Li, X. K. B. M. G. T. L., Liang Wang; Shaddix, C. R. *Energy Fuels* **2015**, *29*, 4328–4338.

(25) Farrow, T. S.; Sun, C.; Snape, C. E. *Journal of Analytical and Applied Pyrolysis* **2015**, *113*, 323 – 331.

(26) Tremel, A.; Haselsteiner, T.; Nakonz, M.; Spliethoff, H. *Energy* **2012**, *45*, 176 – 182.

(27) Riaza, J.; Khatami, R.; Levendis, Y. A.; lvarez, L.; Gil, M. V.; Pevida, C.; Rubiera, F.; Pis, J. J. *Combustion and Flame* **2014**, *161*, 1096 – 1108.

(28) Biagini, E.; Biasci, L.; Marcucci, M. *IFRF report* **2010**, *G 03/y/03*.

(29) Hercog, J.; Tognotti, L. *IFRF report* **2008**, *D 10/y/01*.

(30) Yakhot, O. S. T. S. G. T. . S. C., V. *Physics of Fluids A* **1992**, *4*, 1510 – 1520.

(31) Magnussen, B. F.; Hjertager, B. H. *Symposium International on Combustion* **1977**, *16*, 719–729.

(32) Smith, T.; Shen, Z.; Friedman, J. N. *Journal of Heat Transfer* **1982**, *104*, 602 – 608.

(33) Erickson, C. A. *Joint ASME/JSME Pressure Vessels and Piping Conference* **1982**, *104*, 602 – 608.

List of Figures

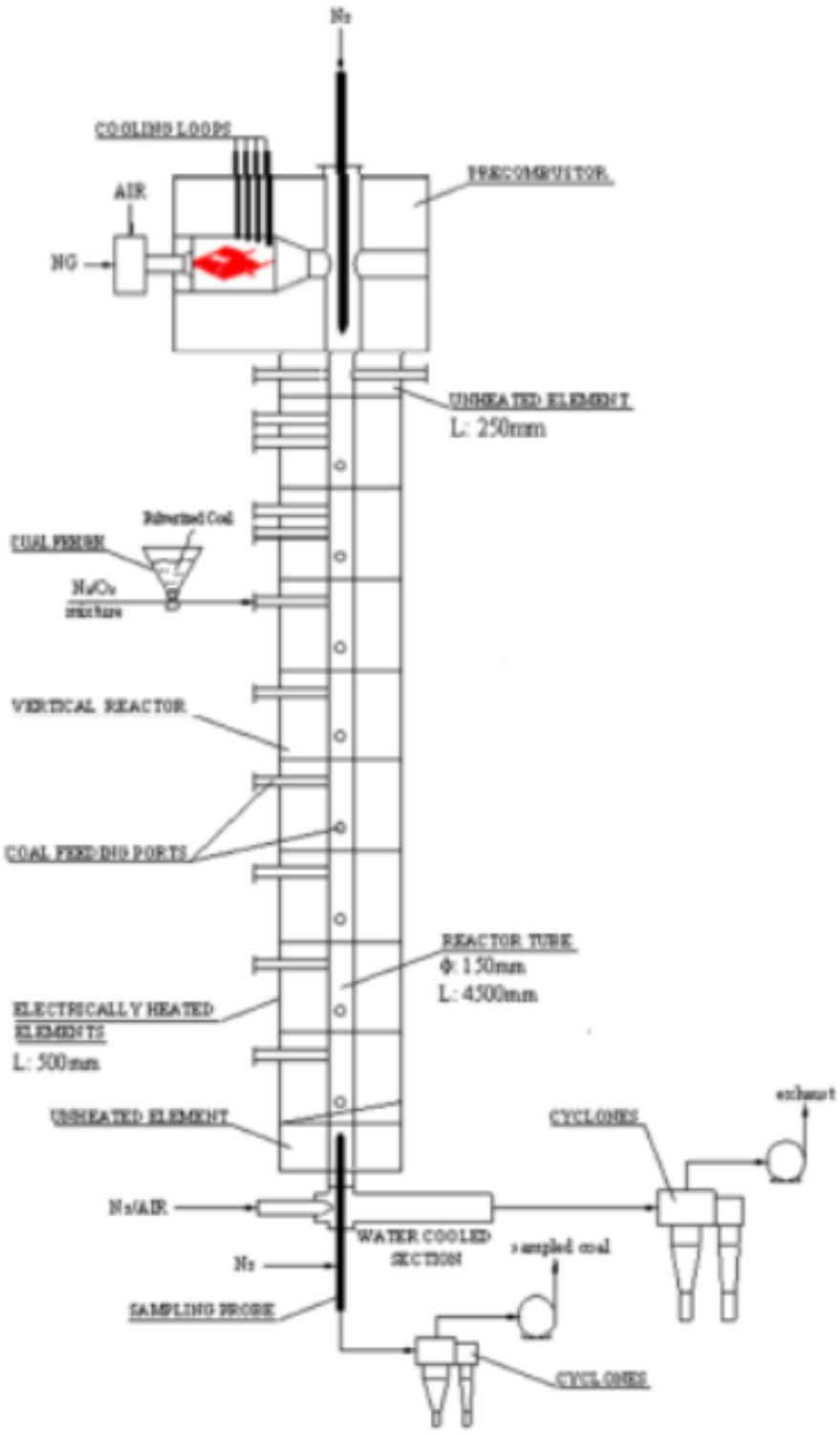

Figure 1: Scheme of the entrained flow reactor.

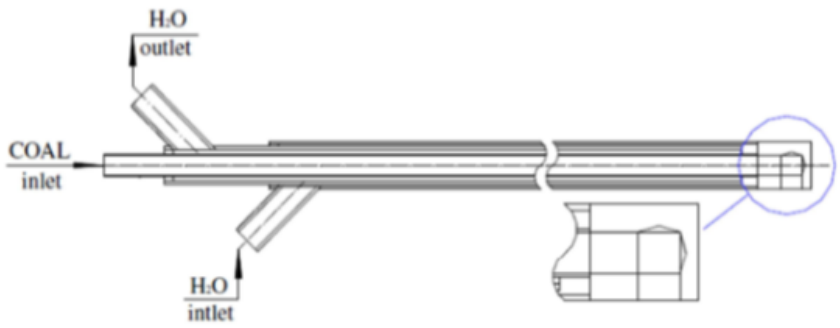

Figure 2: Scheme of the feeding probe.

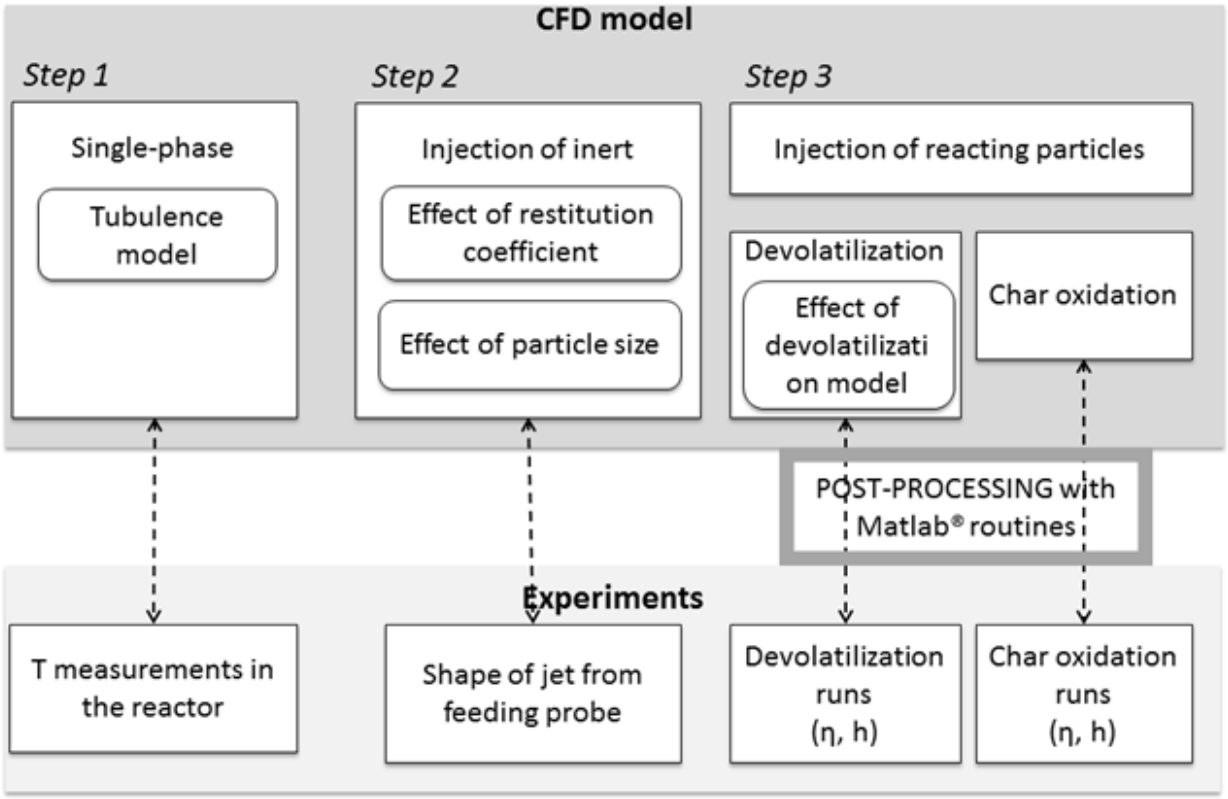

Figure 3: Scheme of the modeling approach.

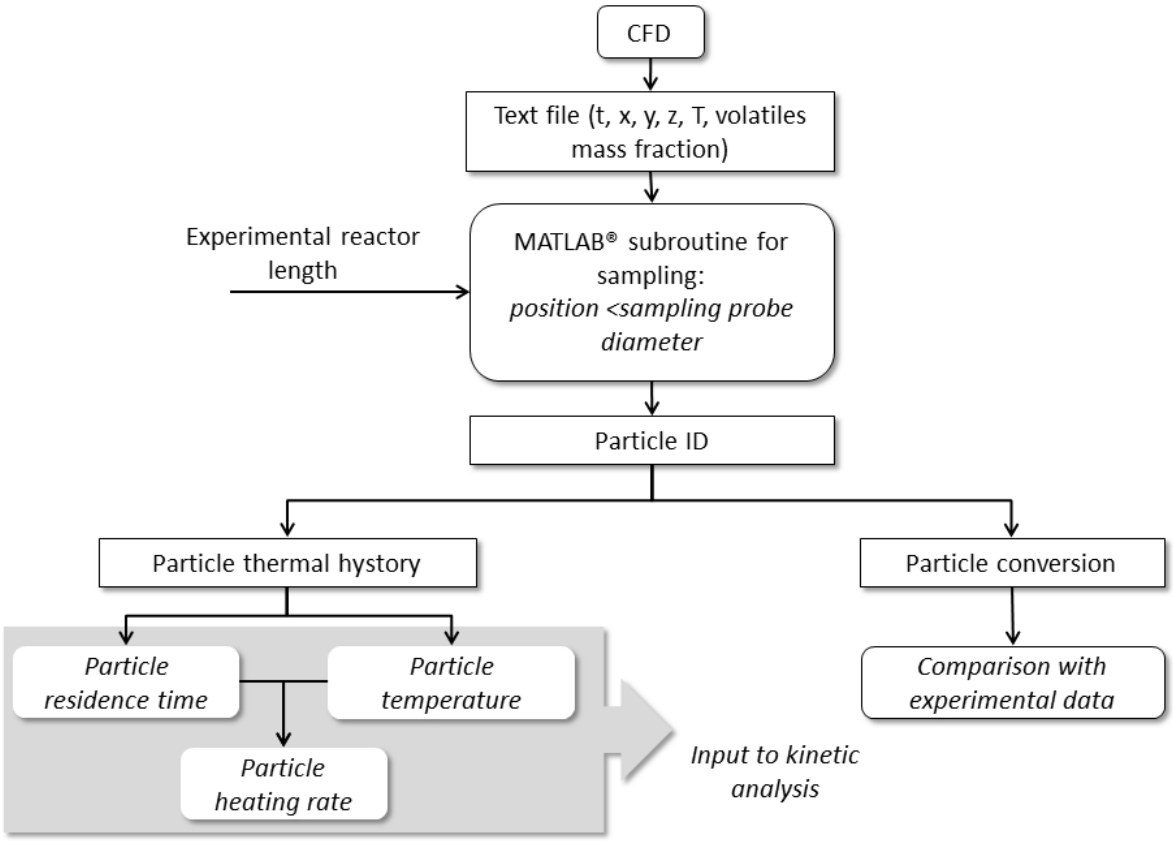

Figure 4: Scheme of post-processing procedure.

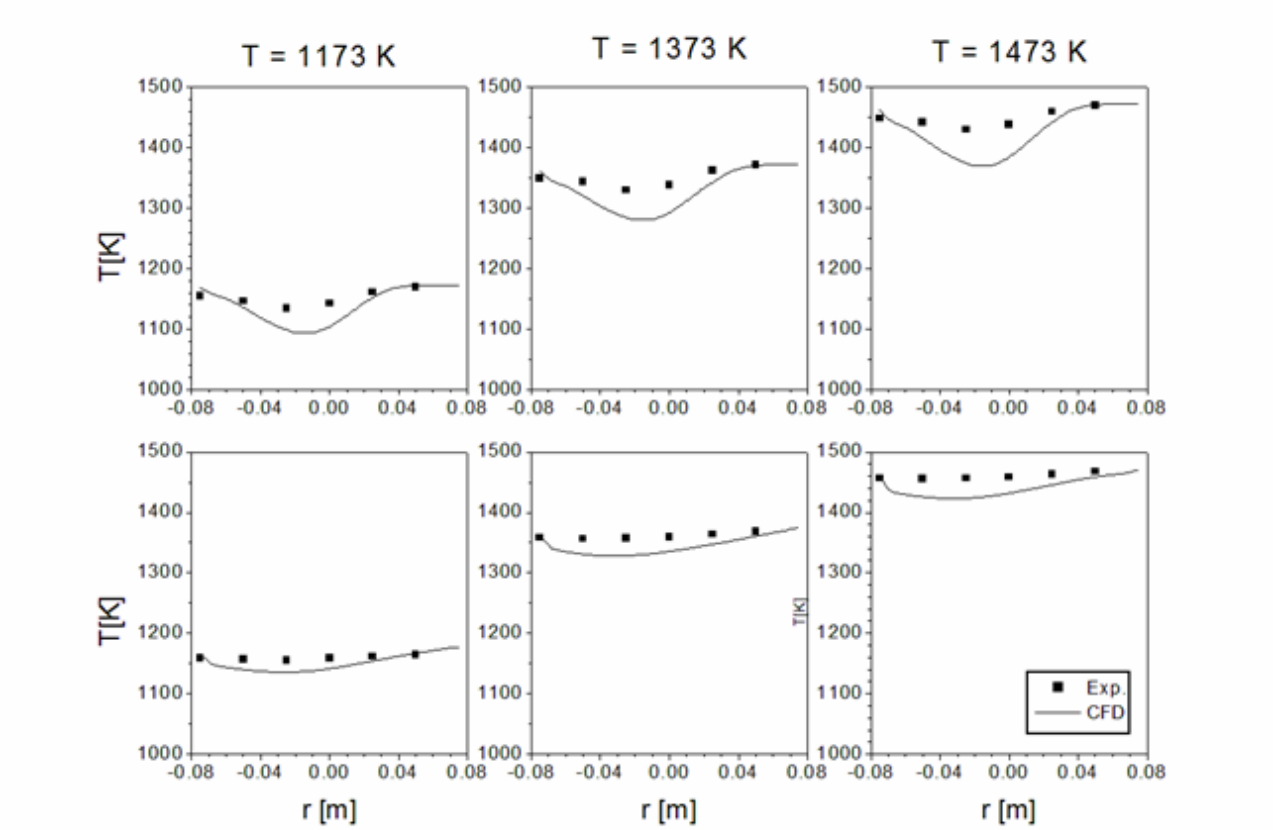

Figure 5: Predicted and measured temperature profiles taken (top) 0.5 m and (bottom) 1.01 m below of the feeding probe for different reactor nominal temperature, i.e. $T_R = 1173$, 1373 and 1473 K.

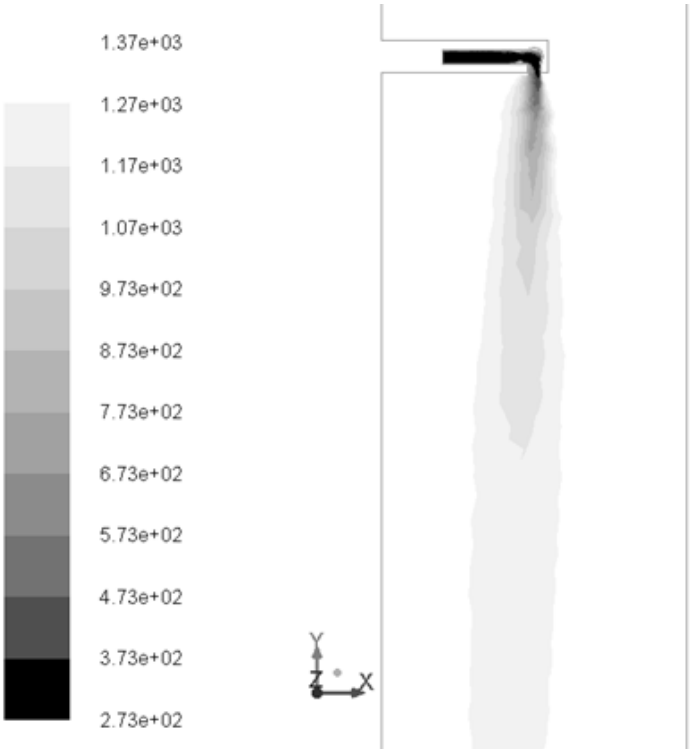

Figure 6: Temperature (in K) distribution in the longitudinal section of the IPFR for $T_R =$ 1373K.

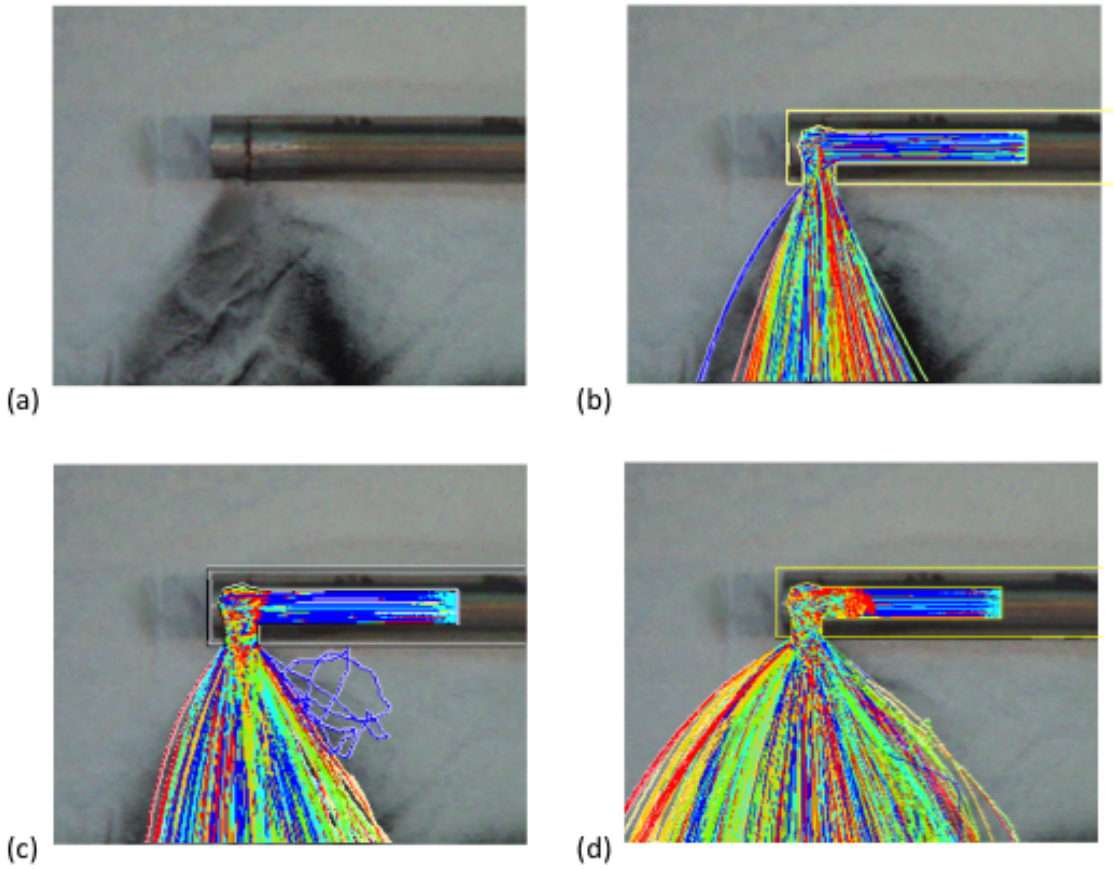

Figure 7: Experimental image of the jet of coal particles (a) and coal trajectories predicted with (a) $R = 0.3$, (b) $R = 0.6$ and (c) $R = 1$ using non-reacting simulations

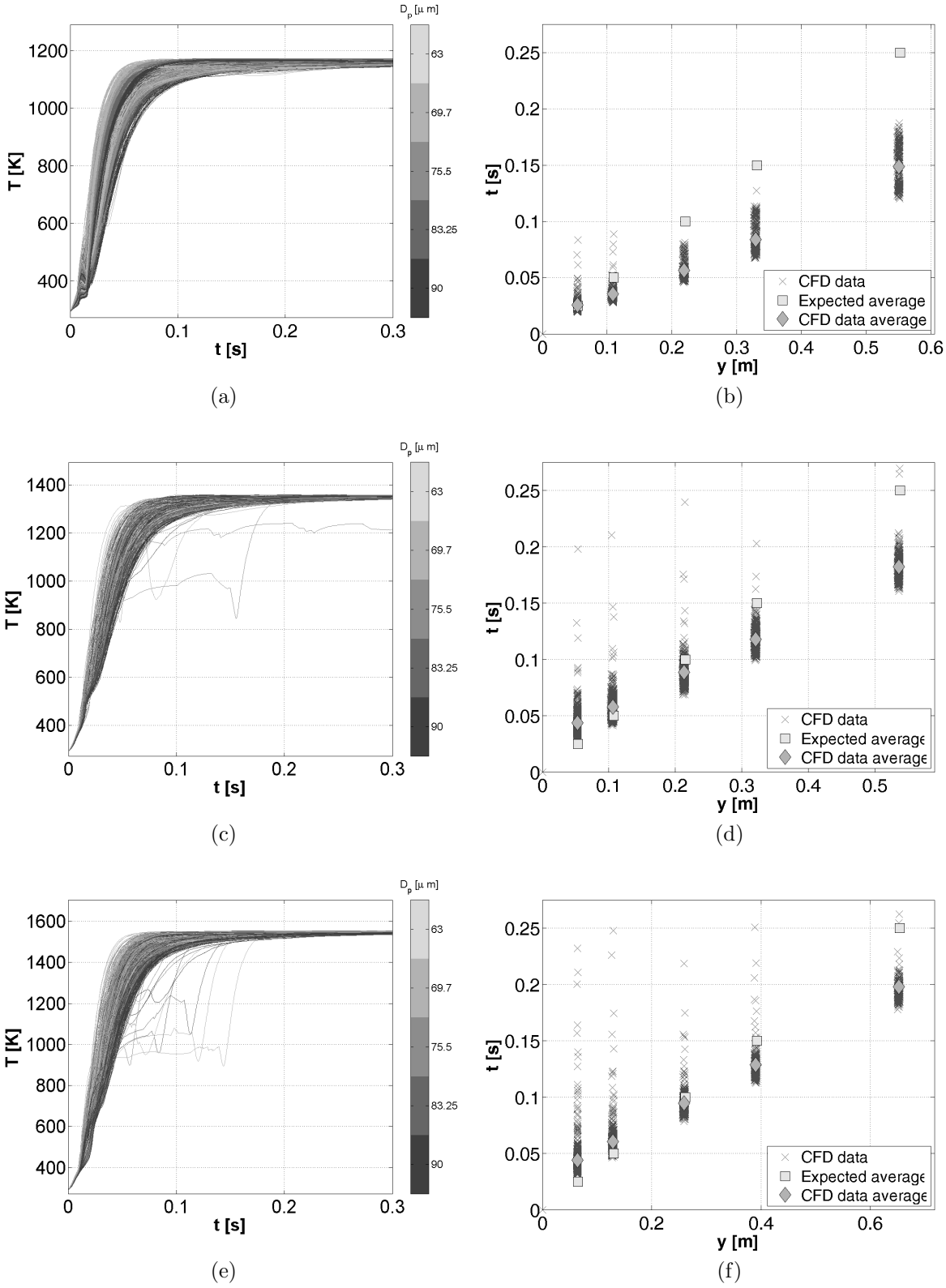

Figure 8: (a,c,e) Temperature as a function of residence time and (b,d,f) residence time as a function of reactor length as predicted injecting inert particles with (a,b) $T_R = 1173$ K, (c,d) $T_R = 1373$K, (e,f) $T_R = 1573$ K

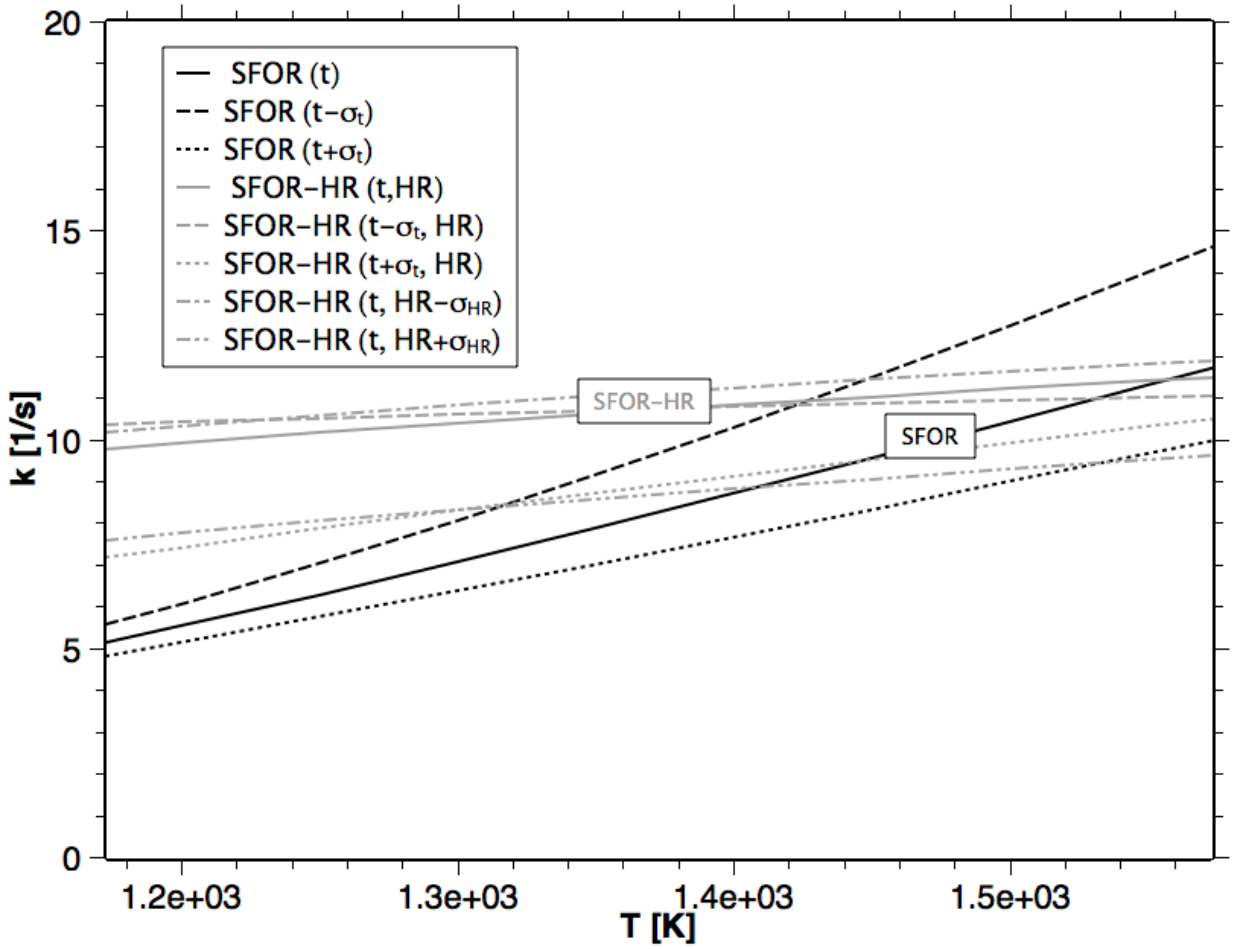

Figure 9: Kinetic constant k as a function of temperature T as calculated for SFOR and SFOR-HR with average residence time t and heating rate HR as well as considering their variance.

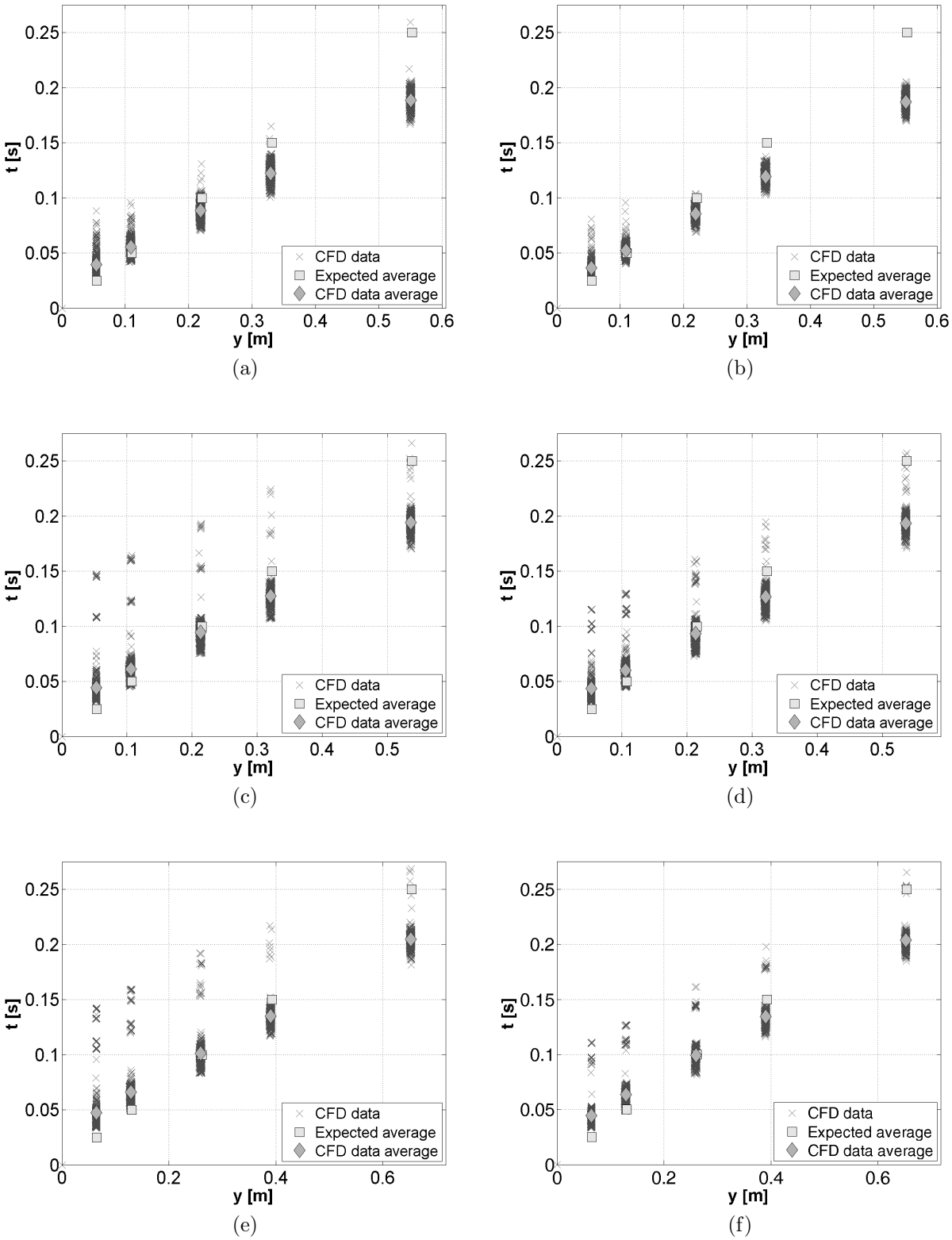

Figure 10: Residence time as a function of sample length for (a,b) $T_R = 1173$ K, (c,d) $T_R = 1373$K, (e,f) $T_R = 1573$ K as evaluated with the (a,c,e) SFOR and (b,d,f) SFOR-HR models.

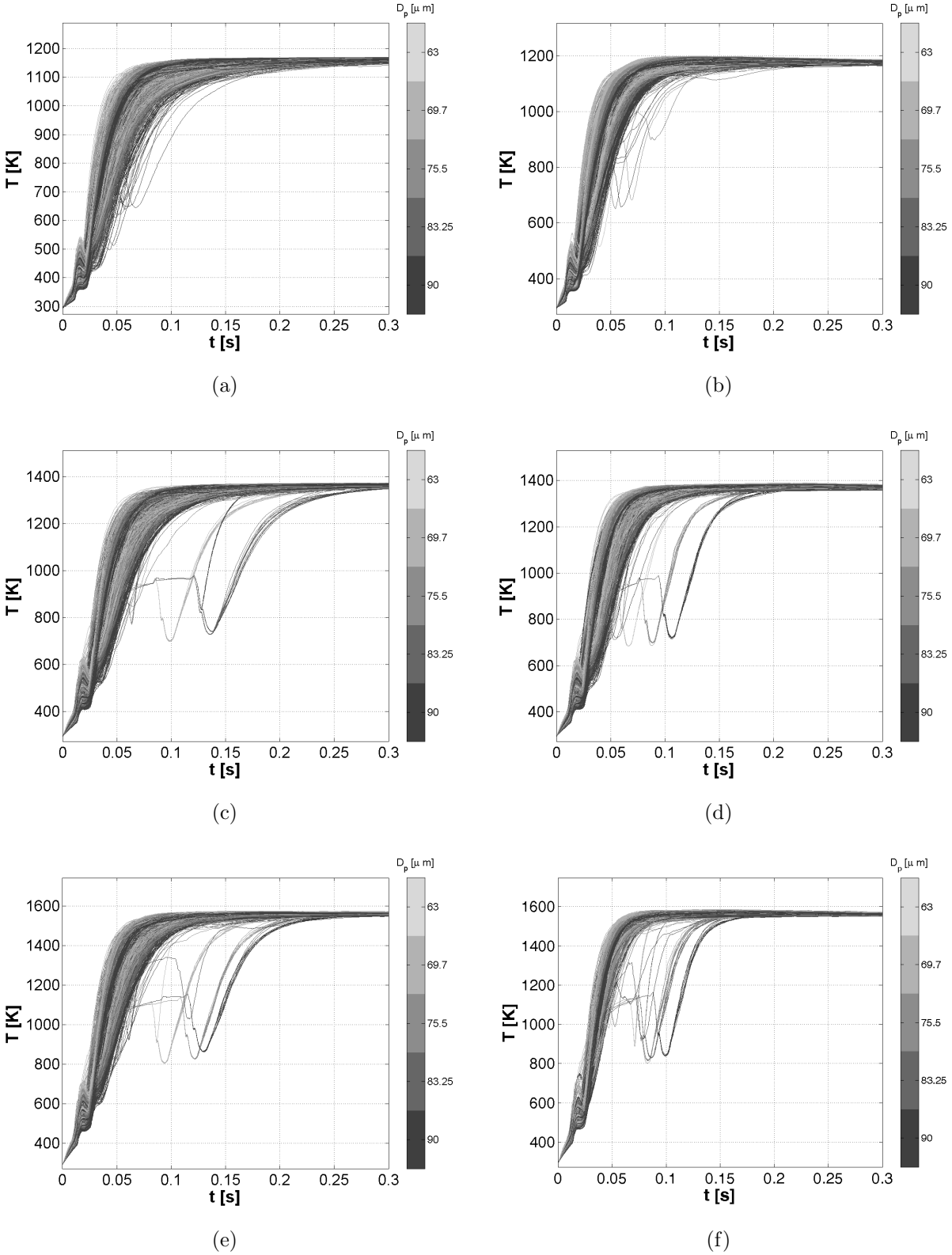

Figure 11: Temperature as a function of residence time for (a,b) $T_R = 1173$ K, (c,d) $T_R = 1373$K, (e,f) $T_R = 1573$ K as evaluated with the (a,c,e) SFOR and (b,d,f) SFOR-HR models.

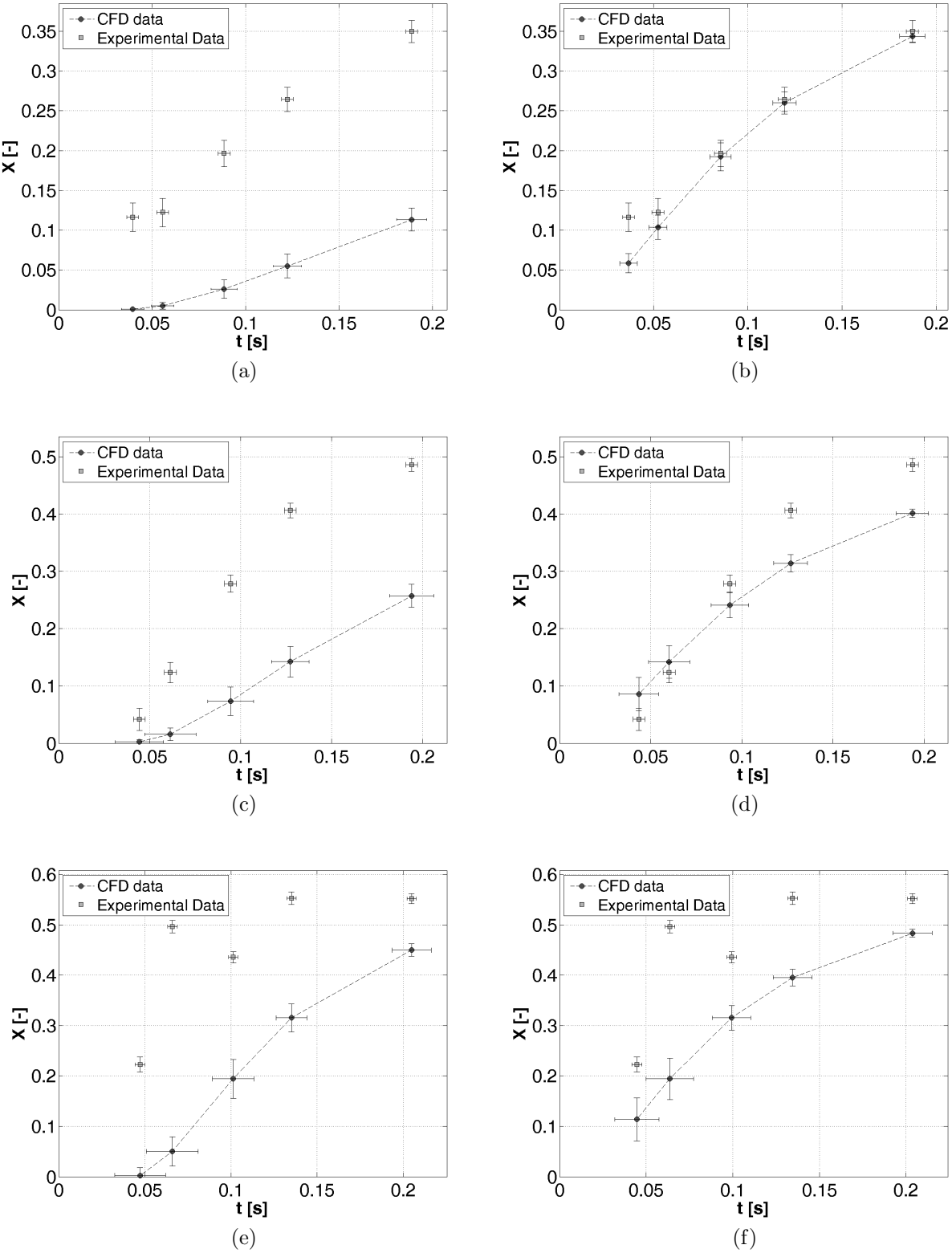

Figure 12: Conversion as a function of residence time for (a,b) $T_R = 1173$ K, (c,d) $T_R = 1373$K, (e,f) $T_R = 1573$ K as evaluated with the (a,c,e) SFOR and (b,d,f) SFOR-HR model.

List of Tables

Table 1: Proximate and ultimate analysis of the Sebuku Indonesian coal.

HUM [%]	VM [%db]	FC [%db]	Ash [%db]	C [%db]	H [%db]	N [%db]	S [%db]	O [%db]	LHV [$MJ/kgdb$]
8.84	40.30	47.95	11.75	62.75	4.56	1.27	0.48	19.09	27.03

Table 2: Flow rates for experimental runs

	precombustor			reactor		
T_r [K]	GN [Nm^3/hr]	air [Nm^3/hr]	N_2 [Nm^3/hr]	CO_2 carrier [Nm^3/hr]	coal [g/hr]	N_2 quench [Nm^3/hr]
1173	2.1	22.0	11	0.6	130	19
1373	2.9	26.3	0	0.5	120	22
1573	3.3	31.0	0	0.5	120	24

Table 3: Average heating rates and their standard deviations obtained by CFD with inert particles and reactive particles using SFOR and SFOR-HR devolatilization models.

	Inert particles		SFOR		SFOR-HR	
	HR [K/s]	σ_{HR} [K/s]	HR [K/s]	σ_{HR} [K/s]	HR [K/s]	σ_{HR} [K/s]
T_R=1173 K	13164	2648	11502	3254	12870	3309
T_R=1373 K	12408	2442	13439	4135	16559	5045
T_R=1573 K	19421	2488	16303	5184	17701	5373

Table 4: Average residence times and their standard deviations obtained by CFD with inert and reactive particles using SFOR and SFOR-HR model for different reactor temperatures: (a) $T_R = 1173$ K, (b) 1373 K and (c) 1573 K.

(a)

Inert particles		SFOR		SFOR-HR	
t [s]	σ_t [s]	t [s]	σ_t [s]	t [s]	σ_t [s]
0.0257	0.0041	0.0397	0.0060	0.0366	0.0047
0.0355	0.0050	0.0557	0.0061	0.0523	0.0048
0.0563	0.0064	0.0885	0.0070	0.0855	0.0056
0.0838	0.0119	0.1223	0.0075	0.1193	0.0062
0.1487	0.0183	0.1888	0.0080	0.1873	0.0068

(b)

Inert particles		SFOR		SFOR-HR	
t [s]	σ_t [s]	t [s]	σ_t [s]	t [s]	σ_t [s]
0.0439	0.0324	0.0444	0.0134	0.0435	0.0108
0.0589	0.0337	0.0614	0.0141	0.0601	0.0112
0.0903	0.0385	0.0945	0.0126	0.0934	0.0103
0.1205	0.0095	0.1274	0.0103	0.1268	0.0093
0.1866	0.0168	0.1941	0.0121	0.1936	0.0088

(c)

Inert particles		SFOR		SFOR-HR	
t [s]	σ_t [s]	t [s]	σ_t [s]	t [s]	σ_t [s]
0.0416	0.0190	0.0472	0.0147	0.0446	0.0126
0.0554	0.0118	0.0660	0.0150	0.0636	0.0137
0.0844	0.0136	0.1013	0.0121	0.0993	0.0117
0.1128	0.0137	0.1351	0.0089	0.1345	0.0111
0.1714	0.0298	0.2048	0.0114	0.2037	0.0113

Table 5: Kinetic parameters A and E obtained for SFOR and SFOR-HR, and errors due to uncertainty on residence time and heating rate.

	SFOR			SFOR-HR			SFOR-HR		
	t-σ_t	t	t+σ_t	t-σ_t	t	t+σ_t	HR-σ_{HR}	HR	HR+σ_{HR}
A [1/s]	246.89	131.22	84.20	13.26	18.46	31.71	18.72	18.46	19.03
E [J/kmol]	$3.70\ 10^7$	$3.16\ 10^7$	$2.79\ 10^7$	$2.42\ 10^6$	$6.22\ 10^6$	$1.45\ 10^7$	$5.94\ 10^6$	$6.22\ 10^6$	$8.96\ 10^6$